Impact of sensor placement in soil water estimation ⋆

Erfan Orouskhani * **Soumya R. Sahoo** * **Bernard T. Agyeman** *
Song Bo * **Jinfeng Liu** *,**

* *Department of Chemical and Materials Engineering, University of Alberta, Edmonton, AB T6G 1H9, Canada*
** *Email: jinfeng@ualberta.ca.*

Abstract: Soil moisture estimation is an essential element in the implementation of a closed-loop irrigation system. The determination of the best locations to install the sensors such that good state estimation can be obtained is an important problem. In our previous work, this issue has been addressed by employing the modal degree of observability based on extensive simulations. It was found that optimally placed sensors can lead to much-improved soil moisture estimation performance. However, it is unclear whether the significantly improved estimation performance can still be observed in actual applications. In this work, we consider an actual agricultural field in Lethbridge, Alberta, Canada, and study the impact of sensor placement in soil water estimation. Soil moisture measurements from 42 soil moisture sensors installed at different depths were collected for one growing season. First, a three-dimensional agro-hydrological model with heterogeneous soils is developed. Then, a state estimator designed based on the extended Kalman filter (EKF) is adopted to estimate the soil water content. Subsequently, we apply the modal degree of observability to the three-dimensional system and determine where the best sensor locations are. Different scenarios are considered to estimate the soil water content and the estimation results are analyzed for all the scenarios.

Keywords: Sensor placement; degree of observability; state estimation; extended Kalman filter, Richards equation.

1. INTRODUCTION

Freshwater scarcity is becoming a serious issue worldwide primarily due to population growth, climate change, and increasing pollution (UNESCO (2009)). Of the total amount of freshwater, about 70% is consumed in the agricultural activities, with the main consumer being irrigation (WWAP (2018)). Currently, the water-use efficiency in irrigation is estimated to be 60% due to poor irrigation strategies (UNESCO (2009)). In order to mitigate the freshwater supply crisis, the water-use efficiency in agriculture irrigation needs to be improved. One promising solution to improve the water-use efficiency is to use a closed-loop irrigation system where a controller uses real-time field conditions to make the best irrigation decisions (Nahar et al. (2019)). However, in implementing the closed-loop irrigation system, the soil moisture information of the entire field which should be fed back to the controller is required. On the other hand, the agriculture fields usually are of large scale and installing sensors in the whole field is impractical. Therefore, the main barrier in implementing the closed-loop irrigation system is the lack of soil moisture measurements. To address this issue, using state estimation techniques which reconstruct full states information based on the measurements of a small number of sensors have been proposed. Due to the nonlinearity of the field model, the nonlinear state estimators such as extended Kalman filter (Reichle et al. (2002); Agyeman et al. (2021)), ensemble Kalman filter (Zhang et al. (2018)), and particle filter (Pasetto et al. (2012); Montzka et al. (2011)) have been typically used to address the problem of soil moisture estimation in the literature.

In the above studies, the optimal sensor placement has not been considered. Because of the limited number of sensors in the agricultural fields, the determination of the best locations to install the sensors such that good state estimation can be obtained is an important problem. In Nahar et al. (2017), Nahar and co-authors proposed to use the observability analysis to find the optimal sensor locations. However, the applicability of this method was restricted to one-dimensional systems. Then, in our recent work, (Sahoo et al. (2019)), the optimal sensor placement problem has been addressed by employing the modal degree of observability. It was demonstrated the optimally placed sensors can improve soil moisture estimation performance. However, it is unclear whether the optimal sensor placement can significantly improve the estimation performance in actual applications. Moreover, in all the above studies, homogeneous soil parameters or simple arrangements of different soil types have been considered.

In this work, we investigate the impact of sensor placement in soil water estimation of agro-hydrological systems with heterogeneous soils for an actual field. The actual field studied in this work is located in Lethbridge, Alberta,

⋆ Financial support from Natural Sciences and Engineering Research Council of Canada (NSERC) and Alberta Innovates is gratefully acknowledged

Fig. 1. The layout of the studied field

Canada. First, 42 soil moisture sensors were installed at different depths of the field to collect the soil moisture measurements for one growing season. Next, a three-dimensional agro-hydrological model with heterogeneous soil parameters of the studied field is developed. Then, the extended Kalman filter (EKF) is chosen as a state estimator to estimate the soil water content. Subsequently, we apply the modal degree of observability to the three-dimensional system to determine the best locations of the sensors. Finally, estimation results are obtained and analyzed to investigate the effect of sensor placement on the performance of soil moisture estimation in actual applications.

2. DESCRIPTION OF THE STUDIED FIELD

The agricultural field studied in this work is located in Lethbridge, Alberta, Canada. The layout of the field is shown in Figure 1. The field is a circular one with a radius of about 50 meters. The depth of the field is 75 cm in the simulations of this work. The soil texture consists of three types of soil: clay, silt, and sand. Each area of the field has a different percentage of the soil types that makes the soil profile heterogeneous. Thus, the soil profile of the field has different properties at various zones. In the studied field, a centre pivot is used as the irrigation implementing system. In irrigation time, the center pivot rotates at a speed of 0.011 m/s.

The soil profiles at 60 points of the studied field were sampled. The soil profile data will be used in Section 3.2 to interpolate the soil parameters of the entire field. Moreover, 42 watermark sensors were installed in the field at different depths (14 sensors at the depth of 25 cm, 14 sensors at the depth of 50 cm, and 14 sensors at the depth of 75 cm, below the surface) to measure the pressure head of these locations. The measurements were collected every 60 minutes from June 19 to August 13, 2019. Some irregular features in the real dataset, increase the model plant mismatch and cause the overall state estimation more challenging. This data will be used in Section 7 to estimate the soil moisture of the entire field through a state estimator. The precipitation data of the studied field was obtained from the Alberta Climate Information Service (ACIS) website (https://agriculture.alberta.ca/acis/). Figure 2 shows the precipitation data on a daily basis for the period under investigation.

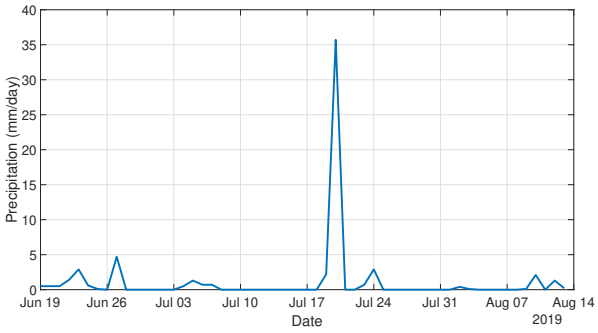

Fig. 2. Daily precipitation data of the studied field during the period under investigation

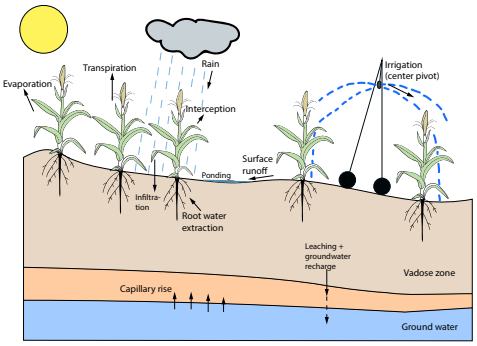

Fig. 3. An agro-hydrological system (Bo et al. (2020))

3. MODELING OF THE WATER DYNAMICS OF THE STUDIED FIELD

3.1 Agro-hydrological system description

An agro-hydrological model characterizes the hydrological cycle between the soil, the water, the atmosphere, and the crop. Figure 3 provides an illustration of an agro-hydrological system (Bo et al. (2020)). The dynamics of soil water can be modeled using the Richards' equation as follows (Richards (1931)):

$$\frac{\partial \theta}{\partial t} = C(h)\frac{\partial h}{\partial t} = \nabla \cdot (K(h)\nabla(h+z)) - S \qquad (1)$$

where h (m) is the pressure head, θ $(m^3 m^{-3})$ is the volumetric water content, t (s) is time, z (m) is the spatial coordinate, $K(h)$ (ms^{-1}) is the unsaturated hydraulic water conductivity, $C(h)$ (m^{-1}) is the capillary capacity, and S $(m^3 m^{-3} s^{-1})$ denotes the sink term, representing the root water extraction rate. In equation (1), the soil hydraulic functions $\theta(h)$ and $K(h)$ can be obtained by the Mualem-van Genucthen model (Van Genuchten (1980)):

$$\theta(h) = \theta_r + (\theta_s - \theta_r)\left[\frac{1}{1+(-\alpha h)^n}\right]^{1-\frac{1}{n}} \qquad (2)$$

$$K(h) = K_s\left[(1+(-\alpha h)^n)^{-\left(\frac{n-1}{n}\right)}\right]^{\frac{1}{2}} \times \left[1-\left[1-\left[(1+(-\alpha h)^n)^{-\left(\frac{n-1}{n}\right)}\right]^{\frac{n}{n-1}}\right]^{\frac{n-1}{n}}\right]^2 \qquad (3)$$

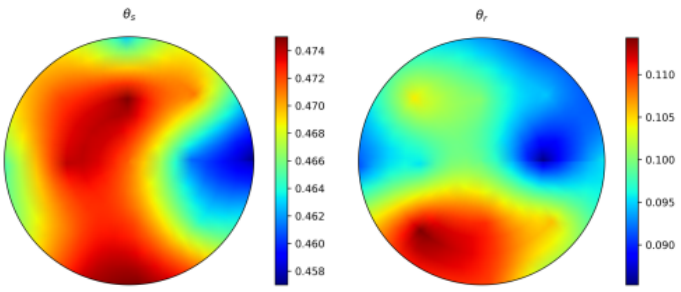

(a) θ_s (m^3m^{-3}) (b) θ_r (m^3m^{-3})

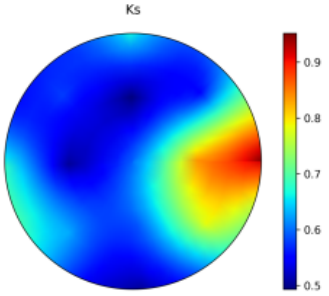

(c) K_s $(cmhr^{-1})$

Fig. 4. Soil texture of the surface of the investigated field

where θ_s (m^3m^{-3}), θ_r (m^3m^{-3}), K_s (ms^{-1}) are the saturated volumetric moisture content, residual moisture content and saturated hydraulic conductivity, respectively. n and α are curve-fitting soil hyrdraulic properties.

3.2 Interpolation of soil parameters

The parameters $\theta_s, \theta_r, K_s, \alpha$, and n form a set of soil parameters that determine the soil properties of the field. Due to the heterogeneity of the soil in the studied field, the soil parameters are different at different points of the field. In fact, each point in the field which corresponds to a node in the discretized model has its own set of soil parameters. These soil parameters are unknown and need to be obtained. In this work, we use the Kriging interpolation method (Matheron (1963)) to estimate the soil parameters of the entire field. We first used the 60 soil samples of the studied field and determined the soil texture type of the sampled points by measuring the percentage of the clay, silt, and sand soils existing in the samples. Next, we obtained the set of soil parameters for these sampling points based on the composition of the soil types (Carsel et al. (1988)). Subsequently, we used the soil parameters of these 60 sampled points as the measurements in the Kriging interpolation method to interpolate the soil parameters of the entire field. Figure 4 shows the interpolated soil parameters of the surface of the studied field. The results show that the soil parameters of the field are heterogeneous.

3.3 Polar form of Richards' equation

In this paper, the center pivot is considered as the irrigation implementing system in the studied field. In order to model the circular movement of the centre pivot, Richards' equation is expressed in cylindrical coordinates as follows (Agyeman et al. (2021)):

$$C(h)\frac{\partial h}{\partial t} = \frac{1}{r}\frac{\partial}{\partial r}\left[rK(h)\frac{\partial h}{\partial r}\right] + \frac{1}{r}\frac{\partial}{\partial \theta}\left[\frac{K(h)}{r}\frac{\partial h}{\partial \theta}\right] + \frac{\partial}{\partial z}\left[K(h)\left(\frac{\partial h}{\partial z}+1\right)\right] - S \quad (4)$$

where r, θ, z represent the radial, azimuthal, and axial directions, respectively.

3.4 Model discretization

Since the polar form of the Richards' equation is a non-linear partial differential equation, numerical solutions are needed to solve this equation. In (Agyeman et al. (2021)), the two point central finite difference scheme is employed to discretize the PDE with respect to the spatial variables (r, θ, z). Then, some boundary conditions were imposed to solve the resulting ODE. For example, the symmetry boundary condition $\frac{\partial h}{\partial r}|_C = 0$ at the centre (C) of the field to deal with singularity that occurs at $r = 0$, or the Neuman boundary condition $\frac{\partial (h)}{\partial z}|_T = -1 - \frac{U_{irr}}{K(h)}$ at the top (T) of the field at $z = 0$, to incorporate the irrigation rate $U_{irr}(ms^{-1})$ into the Richards' equation. The same numerical model development and discretization scheme is used in this paper. Specifically, we discretize the field into 6, 40 and 22 nodes in the radial, azimuthal and axial directions, respectively. The head pressure of the soil at these discretized nodes are the states of the system.

3.5 State-space representation of the field model

The field model is expressed in state space form as:

$$\dot{x}(t) = F(x(t), u(t)) + \omega(t) \quad (5)$$

where $x(t) \in \mathbb{R}^{N_x}$ represents the state vector containing $N_x = 5,280$ pressure head values for the corresponding spatial nodes. $u(t) \in \mathbb{R}^{N_u}$ and $\omega(t) \in \mathbb{R}^{N_x}$ represent the input vector and the model disturbances respectively. Specifically, in this work, the sensors directly measure the states of the system and the output vector $y(k)$ is the head pressure (h) at the measured nodes of the field. Thus, the output equation simply represents a matrix (C) indicating which states are measured by the sensors:

$$y(t) = Cx(t) + v(t) \quad (6)$$

where $y(t) \in \mathbb{R}^{N_y}$ and $v(t) \in \mathbb{R}^{N_y}$ respectively denote the measurement vector and the measurement noise. The matrix C is determined by the sensor placement algorithm.

4. OPTIMAL SENSOR PLACEMENT

In order to determine the best locations to install the sensors in the agricultural fields, Sahoo and co-authors proposed to use the modal degree of observability (Sahoo et al. (2019)). They demonstrated the degree of observability tells us how strongly or weakly observable a system is and it can be used as a measure of the optimality of sensor placement. In this paper, we use the algorithm presented in Sahoo's work (Sahoo et al. (2019)). In the following, we summarize this algorithm.

Modal degree of observability which was inspired from the PBH test, analyzes the ability of a sensor node to

estimate other nodes of the system. For a node i at a specific operating point (k), the normalized measure of the modal degree of observability can be calculated by (Gu et al. (2015))

$$O_i^{(k)} = \sum_{j=1}^{n} (1 - \lambda_j^2(A_d^{(k)}))v_{ij}^2 \tag{7}$$

where $A_d^{(k)}$ is the discretized model Jacobian matrix at time k that can be obtained from $A_d^{(k)} = e^{A(k)T}$ when T is the sampling time, and $\lambda_j (j = 1, \ldots, n)$ are the eigenvalues of matrix $A_d^{(k)}$. Based on the definition (Sahoo et al. (2019)), the observability of the system is the highest when the sensors are located at nodes with the highest degree of observability. Thus, the determination of the optimal sensor placement which is based on the maximization of the degree of observability, consists of three steps:

(1) At each operating point (k), calculate the normalized measure of the modal degree of observability $O_i^{(k)}$ for all the system nodes $i, i = 1, \ldots, n$, where n is the total number of the states.
(2) Compute the final modal degree of observability (O_i) for each node as the average value of the modal degree of observability at each operating points.
(3) Order the measures $O_i, i = 1, \ldots, n$, according to their values. The optimal locations to place the sensors are the nodes with the highest O_i values.

In the following, we describe how the above sensor placement algorithm can be applied to the system considered in this work. Firstly, the Backward Differentiation Formulas (BDFs) methods are used to approximate the time derivative in Eq. (5) and obtain the state trajectory $(x(t))$. To implement the BDFs methods, the cvodes integrator in CasAdi (version 3.5.1) are used (Agyeman et al. (2021)). Then, a symbolic approach using CasAdi is employed to calculate the Jacobian matrix (A) which is required in implementation of the optimal sensor placement algorithm. In calculation of Jacobian matrix, the state trajectory obtained from previous step is required at each operating point (k). Finally, we calculate the discretized model Jacobian matrix from $A_d(k) = e^{A(k)T}$ and use it in Eq. (7) to obtain the degree of observability for all nodes of the system at a specific operating point.

Figure 5 represents the modal degree of observability for different nodes of the system considered in this work. From Figure 5, it can be seen that nodes between 240 and 480, located at 65 cm below the surface layer, have relatively higher values of the modal degree of observability around 0.0574, while placing sensors on the surface corresponding to nodes 5040 to 5280 gives the lowest modal degree of observability about 0.0075. Furthermore, the location of the optimal sensor placement is node 244 which has the highest degree of observability value, 0.148.

5. SOIL MOISTURE ESTIMATOR DESIGN

Once the system observability is checked and the optimal sensor placement is found, state estimation can be performed. In this work, we choose the discrete-time EKF to estimate the states. The detail steps are described as follows:

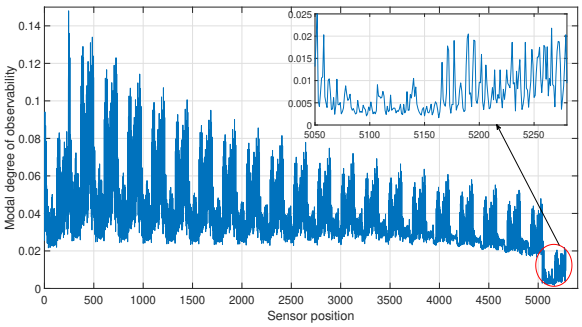

Fig. 5. Modal degree of observability of different nodes

In this work, we rely on extensive simulations to determine the appropriate tuning EKF parameters (matrices P, Q and R). We examine the estimated state trajectories and estimation error for different tuning parameters and choose tuning matrices that improve significantly the estimation performance and result in a smaller estimation error.

6. INITIAL SIMULATION STUDY

In this section, we evaluate the modal degree of observability results for large-scale three-dimensional agro-hydrological systems using state estimation with simulated data. In this study case, the initial condition of the head pressure (x_0) at each state is a random variable between -0.95 m and -0.8 m. The irrigation amount is a constant rate of 3.6 mm/day which is applied to the farm surface in the first 8 hours of each day. The three-dimensional agro-hydrological system obtained in Section 3, is used to simulate the model and obtain the head pressure of the actual system and is further used in the prediction step of the estimator.

In EKF design, 20% mismatch in the initial condition of each state is considered. Twelve head pressure measurements are used to correct the prediction state estimates in the update step of the EKF at each sampling time. Process noise and measurement noise are considered in the simulations and they have zero mean and standard deviations of 1×10^{-6} and 6×10^{-2}, respectively. To verify the effectiveness of the proposed method, two different cases are considered. In the first case, the sensors are placed at 12 nodes with a higher degree of observability, around 1.8056, and the second case is where 12 sensors correspond to nodes with a lower degree of observability, about 0.2937.

Figure 6, represents the trajectories of the actual states and estimated states at some testing nodes. From Figure 6, it can be seen that the estimates by placing the sensors with higher degree of observability converge faster to the actual states. Figure 6(d) compares the total estimation error between case 1 and case 2 and it demonstrates that the root mean square error (RMSE) in case 1 is smaller than case 2 over the simulations. Also, the average RMSE over 6 days simulations in case 1 is 13.15% while in case 2 is 22.71% which shows that the performance of state estimation with optimally sensor placement is significantly improved.

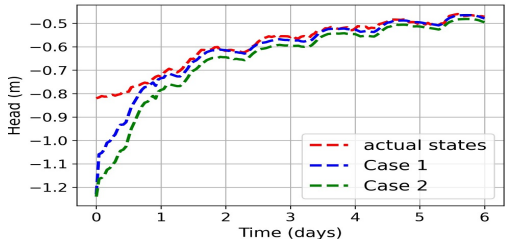

(a) State trajectory at depth = 5 cm

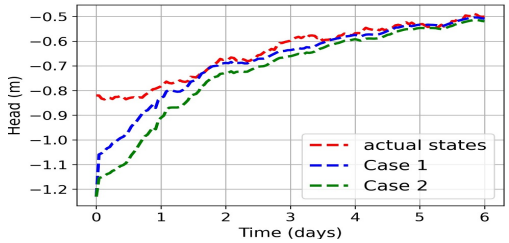

(b) State trajectory at depth = 15 cm

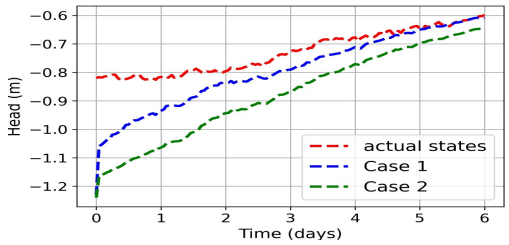

(c) State trajectory at depth = 30 cm

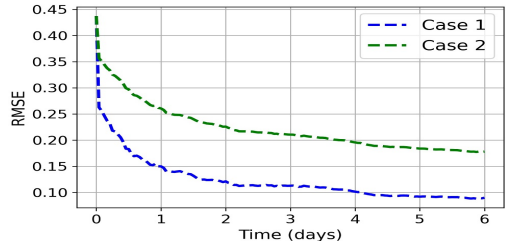

(d) Total estimation error trajectory

Fig. 6. Trajectories of the actual states and estimated states at some testing nodes

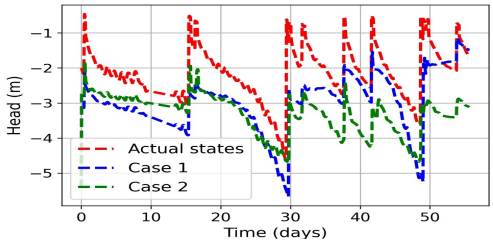

(a) State trajectory at depth = 25 cm

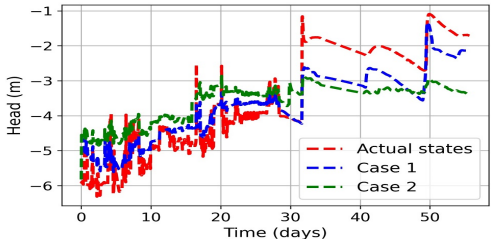

(b) State trajectory at depth = 50 cm

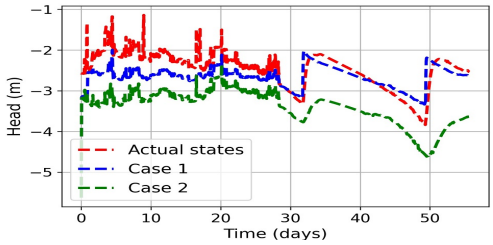

(c) State trajectory at depth = 75 cm

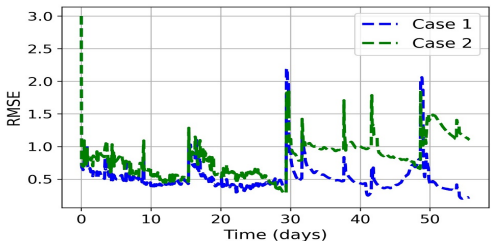

(d) Total estimation error trajectory

Fig. 7. Trajectories of the real states and estimated states at some validation points

7. VALIDATION OF SENSOR PLACEMENT USING REAL DATA

In this section, we investigate the impact of optimal sensor placement in soil water estimation of the studied field using real collected data. The collected data includes the soil water tension of 14 locations at depth of 25 cm, 14 locations at depth of 50 cm, and 14 locations at depth of 75 cm. Before using the collected data as the measurements in the EKF, we have performed some preprocessing steps. First, we converted the soil water tension (Kpa) to the soil head pressure (m). Then, we analyzed the data set to determine which areas of the field have been irrigated over the time period of the experiment. Regarding the sensor placement, the modal degree of observability of 42 measured nodes is obtained and sorted. Then, to verify the effectiveness of the proposed method, two cases are constructed. In case 1, of 42 data points, 15 measured nodes with a higher degree of observability, around 0.8607, are considered as the measurements in EKF. While, in case 2, another 15 measured nodes with a lower degree of observability, about 0.3734, are used as the training points. Also, the rest of the measurements are treated as validation points to compare the real states with estimated states in cases 1 and 2.

Figure 7, represents the trajectories of the real states and estimated states at some validation points. From Figures 7, it can be observed that the estimates by placing the sensors with higher degree of observability converge faster to the actual states. Figure 7(d) compares the total estimation error between case 1 and case 2 and it demonstrates the RMSE in case 1 is smaller than case 2 over the simulations. Also, the average RMSE over 50 days simulation, in case 1, 15.76%, is much smaller than case 2, 37.70%. Therefore, the performance of state estimation

with optimally sensor placement is significantly improved in the actual applications.

In the end, to fairly compare between simulation case study and real data case, we use the normalized RMSE ($NRMES = \frac{RMSE}{\bar{y}}$) which facilitates the comparison between datasets or models with different scales. The NRMSE in the simulation study for case 1 (optimally placed sensors) and case 2 (sensors with a lower degree of observability) over 10 days simulation is about 26.36% and 14.68% respectively, while NRMSE in the real data study for cases 1 and 2 is 28.22% and 15.01% respectively, over the same simulation days. These comparisons demonstrate that optimal sensor placement can significantly improve the performance of state estimation in the actual application and the amount of improvement in the real data case study is very similar to the simulation study case.

ACKNOWLEDGEMENTS

Financial support from NSERC and Alberta Innovates is gratefully acknowledged

REFERENCES

Agyeman, B.T., Bo, S., Sahoo, S.R., Yin, X., Liu, J. and Shah, S.L., (2021). Soil moisture map construction by sequential data assimilation using an extended Kalman filter *Journal of Hydrology*, 598, p.126425, 2021.

Bo, S. and Liu, J., (2020). A decentralized framework for parameter and state estimation of infiltration processes. *Mathematics*, 8(5), 681, 2020.

Carsel, R.F. and Parrish, R.S., (1988). Developing joint probability distributions of soil water retention characteristics. *Water resources research*, 24(5), 755-769.

De Lannoy, G.J., Houser, P.R., Pauwels, V.R. and Verhoest, N.E., (2007). State and bias estimation for soil moisture profiles by an ensemble Kalman filter: Effect of assimilation depth and frequency. *Water resources research*, 43(6).

Entekhabi, D., Nakamura, H. and Njoku, E.G., (1994). Solving the inverse problem for soil moisture and temperature profiles by sequential assimilation of multifrequency remotely sensed observations. *IEEE Transactions on Geoscience and Remote Sensing*, 32(2), 438-448.

Gu, S., Pasqualetti, F., Cieslak, M., Telesford, Q.K., Alfred, B.Y., Kahn, A.E., Medaglia, J.D., Vettel, J.M., Miller, M.B., Grafton, S.T. and Bassett, D.S., (2015). Controllability of structural brain networks. *Nature communications*, 6(1), 1-10.

Heathman, G.C., Starks, P.J., Ahuja, L.R. and Jackson, T.J., (2003). Assimilation of surface soil moisture to estimate profile soil water content. *Journal of Hydrology*, 279(1-4), 1-17.

Hoeben, R. and Troch, P.A., (2000). Assimilation of active microwave observation data for soil moisture profile estimation. *Water Resources Research*, 36(10), 2805-2819.

Houser, P.R., Shuttleworth, W.J., Famiglietti, J.S., Gupta, H.V., Syed, K.H. and Goodrich, D.C., (1998). Integration of soil moisture remote sensing and hydrologic modeling using data assimilation. *Water Resources Research*, 34(12),3405-3420.

Lü, H., Yu, Z., Zhu, Y., Drake, S., Hao, Z. and Sudicky, E.A. (2011). Dual state-parameter estimation of root zone soil moisture by optimal parameter estimation and extended Kalman filter data assimilation. *Advances in water resources*, 34(3), 395-406.

Matheron, G., (1963). Principles of geostatistics. *Economic geology*, 58(8), 1246-1266.

Montzka, C., Moradkhani, H., Weihermüller, L., Franssen, H.J.H., Canty, M. and Vereecken, H., (2011). Hydraulic parameter estimation by remotely-sensed top soil moisture observations with the particle filter. *Journal of hydrology*, 399(3-4), 410-421, .

Nahar, J., Liu, J. and Shah, S.L., (2017). Observability analysis for soil moisture estimation. *IFAC-PapersOnLine*, 50(2), 110-114.

Nahar, J., Liu, J. and Shah, S.L., (2019). Parameter and state estimation of an agro-hydrological system based on system observability analysis. *Computers & Chemical Engineering*, 121, 450-464.

Nahar, J., Liu, S., Mao, Y., Liu, J. and Shah, S.L. (2019). Closed-Loop Scheduling and Control for Precision Irrigation. *Industrial & Engineering Chemistry Research*, 58(26), 11485-11497.

Pasetto, D., Camporese, M. and Putti, M., (2012). Ensemble Kalman filter versus particle filter for a physically-based coupled surface–subsurface model. *Advances in water resources*, 47, 1-13.

Reichle, R.H., Walker, J.P., Koster, R.D. and Houser, P.R., (2002). Extended versus ensemble Kalman filtering for land data assimilation. *Journal of hydrometeorology*, 3(6), 728-740.

Richards, L.A., (1931). Capillary conduction of liquids through porous mediums. *Physics*, 1(5), 318-333.

Sahoo, S.R., Yin, X. and Liu, J., (2019). Optimal sensor placement for agro-hydrological systems. *AIChE Journal*, 65(12), 16795.

UNESCO (United Nations Educational, Scientific and Cultural Organization), (2009). Water in a changing world. The United Nations World Water Development Report 3. *World Water Assessment Programme*.

Van Genuchten, M.T., (1980). A Closed-form equation for predicting the hydraulic conductivity of unsaturated soils. *Soil Science Society of America Journal*, 44(5), 892-898.

Walker, J.P., Willgoose, G.R. and Kalma, J.D., (2001). One-dimensional soil moisture profile retrieval by assimilation of near-surface measurements: A simplified soil moisture model and field application. *Journal of Hydrometeorology*, 2(4) 356-373.

WWAP (United Nations World Water Assessment Programme)/UN-Water. (2018). The United Nations World Water Development Report 2018: Nature-Based Solutions for Water.

Zhang, H., Kurtz, W., Kollet, S., Vereecken, H. and Franssen, H.J.H., (2018). Comparison of different assimilation methodologies of groundwater levels to improve predictions of root zone soil moisture with an integrated terrestrial system model. *Advances in water resources*, 111, 224-238.